

Article

Green, Efficient Detection and Removal of Hg²⁺ by Water-Soluble Fluorescent Pillar[5]arene Supramolecular Self-Assembly

Xiaomei Jiang ¹, Lingyun Wang ^{1,*} , Xueguang Ran ², Hao Tang ¹ and Derong Cao ¹ 

¹ Key Laboratory of Functional Molecular Engineering of Guangdong Province, School of Chemistry and Chemical Engineering, South China University of Technology, 381 Wushan Road, Guangzhou 510641, China; 201910104286@mail.scut.edu.cn (X.J.); haotang@scut.edu.cn (H.T.); drcao@scut.edu.cn (D.C.)

² Institute of Animal Science, Guangdong Academy of Agricultural Sciences, Ministry of Agriculture Key Laboratory of Animal Nutrition and Feed Science in South China, State Key Laboratory of Livestock and Poultry Breeding, Guangzhou 510641, China; rxg59@aliyun.com

* Correspondence: lingyun@scut.edu.cn

Abstract: Developing a water-soluble supramolecular system for the detection and removal of Hg²⁺ is extremely needed but remains challenging. Herein, we reported the facile construction of a fluorescent supramolecular system (H⊃G) in 100% water through the self-assembly of carboxylatopillar[5]arene sodium salts (H) and diketopyrrolopyrrole-bridged bis(quaternary ammonium) guest (G) by host-guest interaction. With the addition of Hg²⁺, the fluorescence of H⊃G could be efficiently quenched. Since Hg²⁺ showed synergistic interactions (coordination and Hg²⁺-cavity interactions with G and H, respectively), crosslinked networks of H⊃G@Hg²⁺ were formed. A sensitive response to Hg²⁺ with excellent selectivity and a low limit of detection (LOD) of 7.17 × 10⁻⁷ M was obtained. Significantly, the quenching fluorescence of H⊃G@Hg²⁺ can be recovered after a simple treatment with Na₂S. The reusability of H⊃G for the detection of Hg²⁺ ions was retained for four cycles, indicating the H⊃G could be efficiently used in a reversible manner. In addition, the H⊃G could efficiently detect Hg²⁺ concentration in real samples (tap water and lake water). The developed supramolecular system in 100% water provides great potential in the treatment of Hg²⁺ detection and removal for environmental sustainability.

Keywords: supramolecular self-assembly; fluorescence sensing; water-soluble pillar[5]arene; mercury(II) detection; diketopyrrolopyrrole



Citation: Jiang, X.; Wang, L.; Ran, X.; Tang, H.; Cao, D. Green, Efficient Detection and Removal of Hg²⁺ by Water-Soluble Fluorescent Pillar[5]arene Supramolecular Self-Assembly. *Biosensors* **2022**, *12*, 571. <https://doi.org/10.3390/bios12080571>

Received: 16 June 2022

Accepted: 22 July 2022

Published: 27 July 2022

Publisher's Note: MDPI stays neutral with regard to jurisdictional claims in published maps and institutional affiliations.



Copyright: © 2022 by the authors. Licensee MDPI, Basel, Switzerland. This article is an open access article distributed under the terms and conditions of the Creative Commons Attribution (CC BY) license (<https://creativecommons.org/licenses/by/4.0/>).

1. Introduction

Mercury ion (Hg²⁺), as one of the most toxic heavy metal ions in the environment and aquatically derived food, has become an important worldwide pollution problem. Hg²⁺ is a neurotoxin and can cause severe adverse effects on human health [1–3]. More importantly, as the most stable and toxic form of mercury, methylmercury in aquatic food chains results in serious damage to the heart, brain, kidneys and immune systems. The maximum contaminant level of Hg²⁺ (10 µg/L) in wastewater discharge was established by World Health Organization (WHO) [4]. Thus far, several functional materials, such as hydrogels, nanoparticles, covalent organic frameworks, porous aromatic frameworks, metal-organic frameworks and others, have shown potential for the possible detection and removal of Hg²⁺ from wastewater [5–10].

Among the various methods for Hg²⁺ recognition, fluorescent self-assembled materials with advanced architectures and stimuli-responsive properties by the supramolecular host-guest interactions have attracted considerable interest [11,12]. They can sensitively and selectively detect targeted analytes with excellent simplicity and good efficiency [13,14]. Pillar[n]arenes are especially popular supramolecular host molecules for their ability to selectively bind different kinds of guests [15,16]. They have a pillar-like framework and multiple

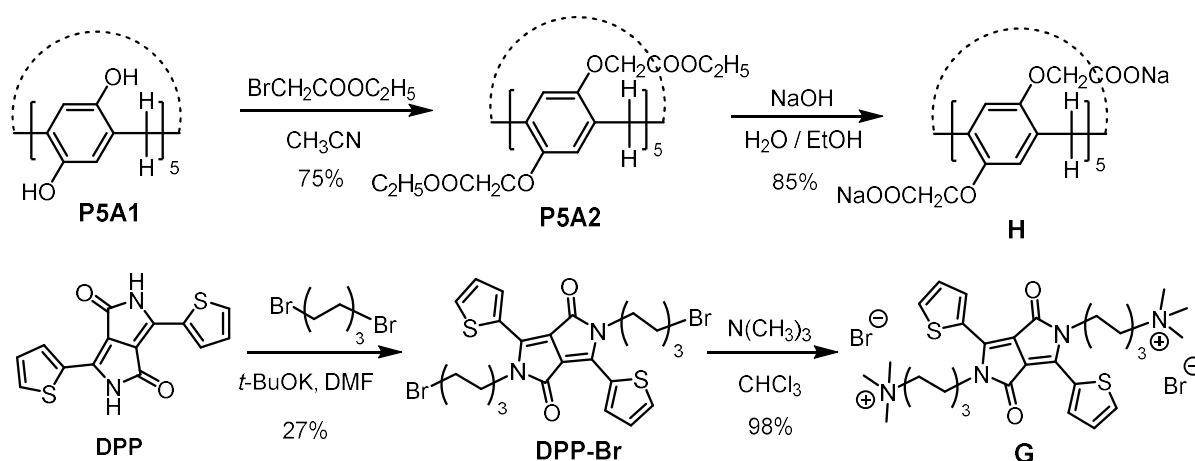
self-assembly driving forces such as hydrophobic/hydrophilic, $\pi \cdots \pi$, C-H $\cdots \pi$, cation $\cdots \pi$ interactions, etc. Thus far, the pillararene-based fluorescent polymer, supramolecular organic framework, gel and supramolecular assembly as Hg^{2+} sensors have been studied by several groups [17–24]. For instance, Yuan's group reported pillar[5]arenes bearing phosphine oxide pendants as Hg^{2+} selective receptors [17]. Wu's and Yang's group developed pillar[5]arene and pillar[6]arene-based aggregation-induced emission-active supramolecular system for detection and removal of Hg^{2+} , respectively [18,21]. Lin's group investigated pillar[5]arene-based polymer and gel as Hg^{2+} fluorescent sensors [22]. Although considerable research efforts for the development of Hg^{2+} supramolecular chemosensors have been made, the participation of organic solvents in these cases is needed, which is unfavorable for Hg^{2+} detection in biological and environmental systems. Moreover, the complicated and tedious synthesis of functional pillararenes is involved. For example, the introduction of Hg^{2+} recognition sites such as thymine, N or S moiety in pillararene is time-costing and cumbersome. More importantly, strong interference from other metal ions is encountered due to the noncovalent interactions sensing mechanism. Therefore, developing water-soluble pillararene-based supramolecular fluorescent materials with excellent Hg^{2+} detection performance in pure water is extremely needed but remains challenging. To the best of our knowledge, a fluorescent supramolecular system in pure water for Hg^{2+} detection and removal has not yet been reported.

Herein, we constructed a supramolecular fluorescent system in pure water, which aims to accomplish the goal of Hg^{2+} sensing and removal in one pot. Some design intentions are listed as follows. (1) Water-soluble carboxylatopillar[5]arene possessed five carboxylate groups on each rim and good binding ability toward guest molecules [25–36], which was selected as a supramolecular host. It may also have cation $\cdots \pi$ and electrostatic interactions with Hg^{2+} . (2) Given that Hg^{2+} possesses a high affinity for N and S, cationic thienyl functionalized diketopyrrolopyrrole (DPP) guest with two six-carbon alkyl chains was selected. It would form a fluorescent supramolecular host–guest system with pillar[5]arene host and possess coordination ability with Hg^{2+} . (3) Through synergistic interactions between Hg^{2+} and host/guest, excellent selectivity and sensitivity would be obtained by fluorescence signal change. By taking these factors into consideration and our research interest in supramolecular fluorescent chemosensors for pollutants [37–40], water-soluble fluorescent pillar[5]arene supramolecular self-assembly was constructed by carboxylatopillar[5]arene sodium salts (**H**) and cationic DPP quaternary ammonium (**G**). The as-prepared supramolecular host–guest system (**H**⊃**G**) showed yellow emission with a multi-layered nanostructure. The synergistic interactions between Hg^{2+} and **H**⊃**G** produce crosslinked networks. The intertwined supramolecular complex **H**⊃**G**@ Hg^{2+} exhibited strong aggregation-caused quenching (ACQ) fluorescence. This enables convenient detection of Hg^{2+} and facile monitoring of the removal procedure. Significantly, the quenching fluorescence of **H**⊃**G**@ Hg^{2+} can be recovered after treatment with Na_2S . As reversible hybrid materials, **H**⊃**G** could be efficiently used in the treatment of Hg^{2+} detection and removal in a reusable manner.

2. Results and Discussion

2.1. Self-Assembly Behavior of **G** in Water

A simpler and modified synthetic method of **H** was developed (Scheme 1). In brief, etherification of OH functionalized pillar[5]arene (**P5A1**) afforded ethoxycarbonylmethoxy-substituted pillar[5]arene (**P5A2**). Then, the hydrolysis of **P5A2** with NaOH by a one-step reaction generated **H** in a high yield. However, a three-steps reaction (hydrolysis, acidification and neutralization) from **P5A2** to **H** was needed in the previous synthesis [36]. In addition, the synthesis of **G** was more straightforward than the reported method [41]. In our case, the N-alkylation and following substitution reaction afforded water-soluble **G**. On the contrary, tedious protection/deprotection reactions of the amino group and HPLC purification of **G** were performed [41]. The ^1H and ^{13}C NMR spectra of **H** and **G** are shown in Figures S1–S4.



Scheme 1. Synthesis of host molecule **H** and guest molecule **G**.

The aqueous solution of **G** exhibited a strong shoulder peak at 507/532 nm and a weak band at 350 nm (Figure S5). Its fluorescence showed a shoulder emission at 560 and 600 nm as well as a weak emission at 650 nm (Figure S5). Since **G** contained a hydrophobic DPP core and two hydrophilic, flexible tails, it tended to form nanoaggregates in water because of the strong π - π stacking among DPP units and the hydrophilic/hydrophobic interaction. ^1H NMR spectrum of **G** proved this assumption, where the chemical shift of hydrogens on thienyl rings of **G** did not split well and showed broad peaks due to aggregation (Figure S3). The SEM images revealed that **G** in water formed tight packing with plenty of nanorods form (Figure 2a,b).

2.2. Host–Guest Complexation Studies in Water

The host–guest complexation was investigated between **G** and **H** in D_2O by ^1H NMR titration spectrum. Figure 1a shows the ^1H NMR spectra of **G** in D_2O recorded in the absence and in the presence of various amounts of **H**. Upon addition of **H**, alkyl protons signals of **G** displayed a clear upfield shift in sharp contrast with pure **G** ($\Delta\delta = -1.76, -0.33, -0.30, -0.37, -1.62$ ppm for protons $\text{H}_f, \text{H}_e, \text{H}_g, \text{H}_h, \text{H}_d$, respectively), indicating the shielding effect of pillar[5]arene cavity and the existence of inclusion complexation. With regard to the ^1H NMR spectrum of **H**, obvious downfield shift ($\Delta\delta = 0.14$ ppm for protons H_2 in phenyl) further confirmed the host–guest inclusion complexation between **H** and **G**. Furthermore, 2D NOESY NMR experiments were performed to investigate the relative spatial positions of protons in this host–guest complex (Figure 1b). It exhibited unequivocal correlation peaks between the signals of H_d - H_i on the alkyl chain of the **G** and H_2 on the phenyl of **H** on viewing the NOESY cross-peaks.

SEM was conducted to characterize the morphology of **H**⊃**G**. As shown in Figure 2c,d, the scattered **H**⊃**G** assemblies with multi-layered nanostructures were observed, which were totally different from that of **G**. We speculated that the formation of the **H**⊃**G** complex was mainly driven by multiple electrostatic interactions, hydrophobic interactions and π - π stacking interactions in aqueous solution. The cooperativity of these noncovalent interactions made **G** be placed inside the cavity of **H** successfully.

The complexation between **H** and **G** also generated UV-vis and emission spectral changes. Upon addition of **H**, the redshifted bands from 507 to 512 and 532 to 538 nm with decreased absorption for **G** were shown, which was ascribed to complexation-induced charge transfer absorption (Figure 3a). Moreover, the absorbance at 350 nm decreased, and the spectrum became broader. As a result, a color change from light pink to pink could be seen, suggesting the formation of a new aggregation state of **H**⊃**G**. At the same time, the addition of **H** led to fluorescence quenching of **G** to some extent (Figure 3b). For example, the absolute fluorescence quantum yield of **G** decreased from 39.1% to 3.7% in the absence and presence of 2 equiv. **H**, respectively. The possible reason can be ascribed to the fact that

multi-layered nanostructures gave closer DPP core stacking and resulted in fluorescence quenching of **G**. At the same time, the zeta potential of -42.43 , 2.13 and -40.49 mV for **H**, **G** and **H** \supset **G** was found, respectively (Figure 3c). Moreover, an obvious Tyndall effect of **H** \supset **G** was shown (Figure 3d). All in all, a host–guest system (**H** \supset **G**) was constructed successfully by adding **H** into **G** aqueous solution, which could induce the change in the aggregation state and fluorescence behavior of **G**.

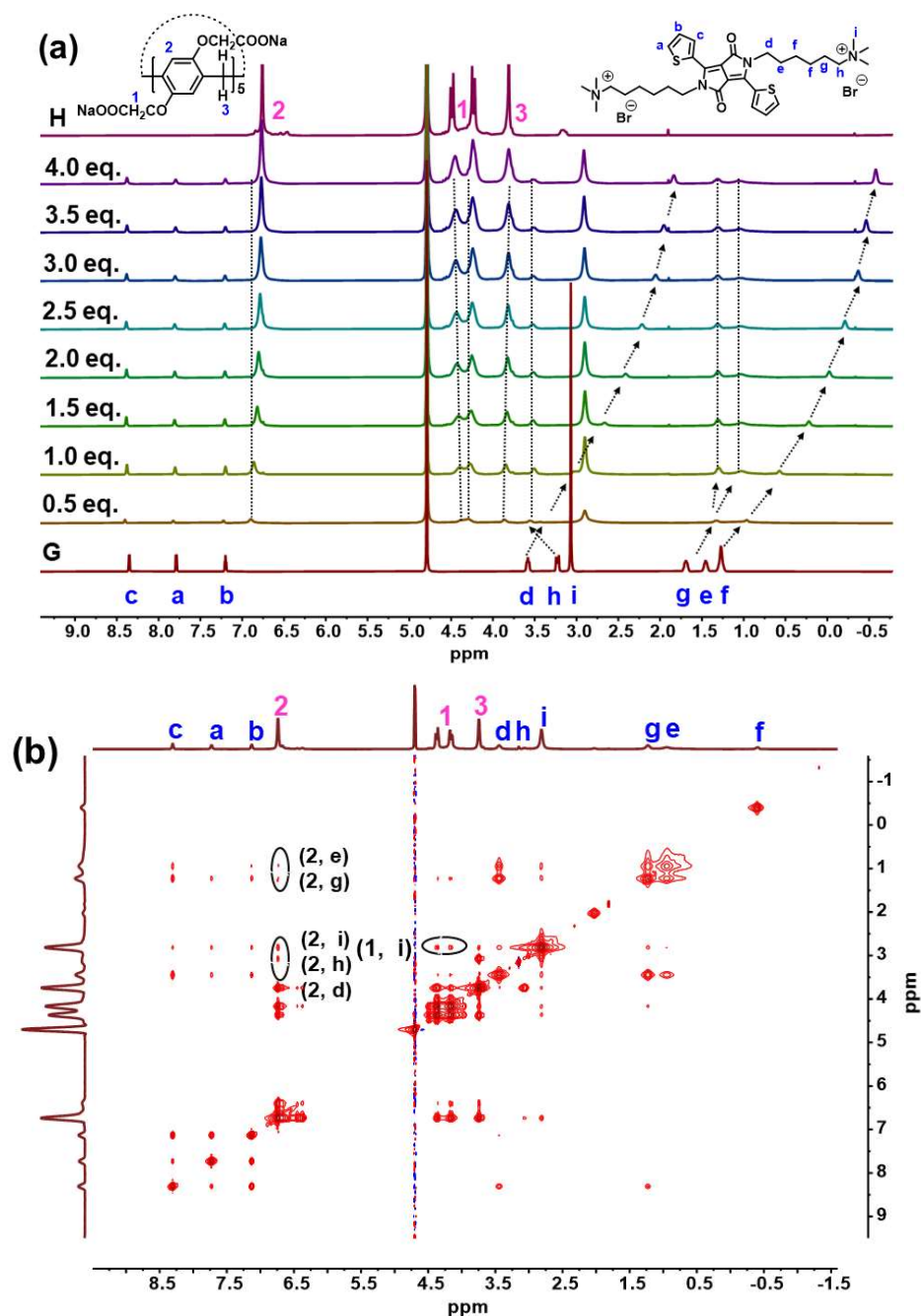


Figure 1. (a) ^1H NMR titration spectra (500 MHz, D_2O) of **G** (8.3 mM) with different equivalents of **H**. The deuterated water has a chemical shift of 4.79 ppm; (b) NOESY spectrum (500 MHz, D_2O) of **H** \supset **G** ($[\text{H}] = 33.2$ mM, $[\text{G}] = 8.3$ mM).

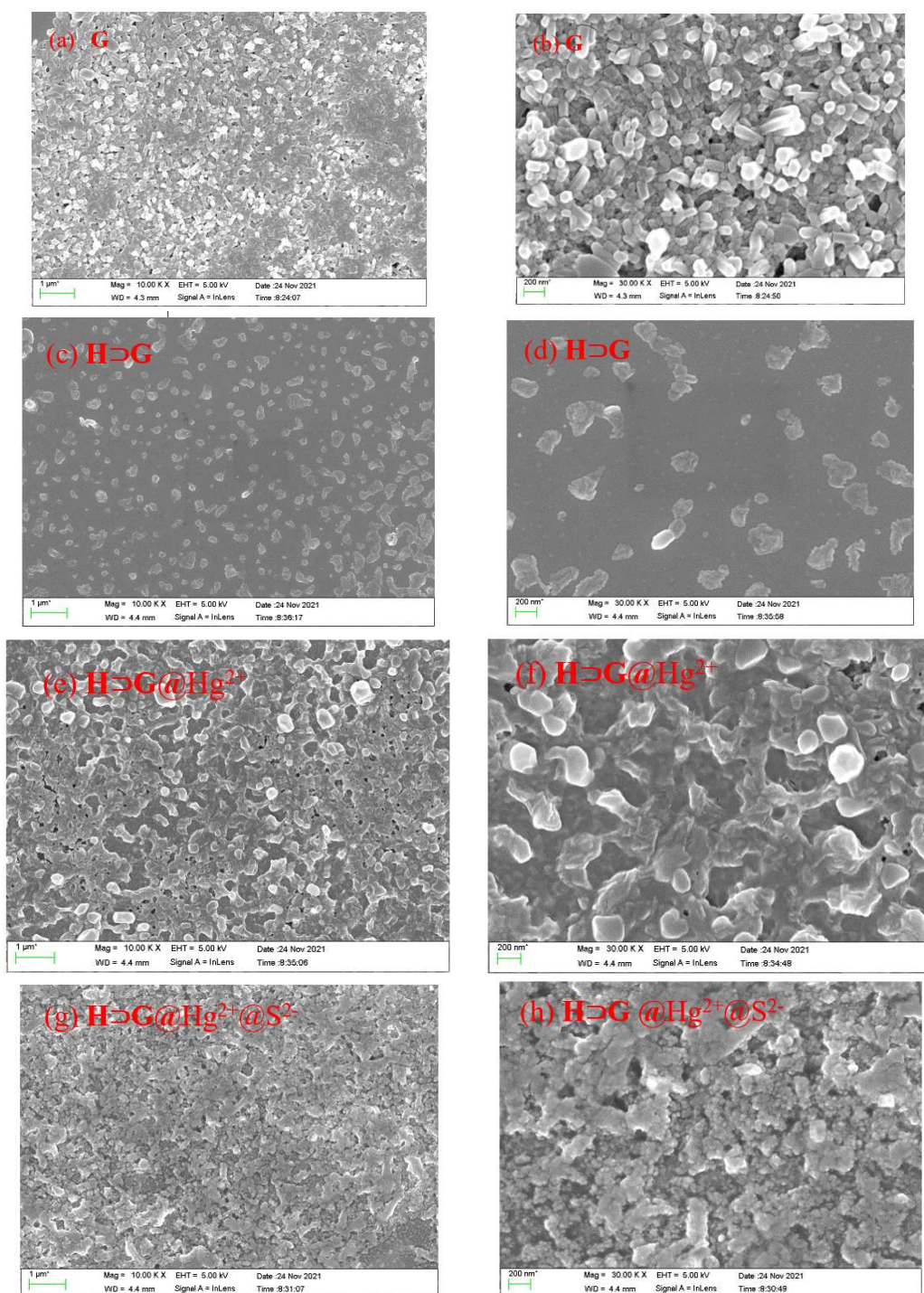


Figure 2. SEM and enlarged SEM images of the G (a,b), H⊃G (c,d), H⊃G@Hg²⁺ (e,f) and H⊃G@Hg²⁺@S²⁻ (g,h). [H] = 2×10^{-5} M, [G] = 10^{-5} M, [Hg²⁺] = 2×10^{-5} M, [S²⁻] = 4×10^{-5} M.

In theory, one G molecule can be complex with two H molecules. Assuming 1:2 inclusion complexation stoichiometry between H and G, the association constants (K_a) could be calculated by using a non-linear least-squares curve-fitting method by use of fluorescence titrations of G with H. The plot of fluorescence change as a function of [H] gave an excellent fit, verifying the validity of the 1:2 inclusion complexation stoichiometry (Figure S6). The K_a value of H⊃G was determined to be $4.8 \times 10^5 \text{ M}^{-2}$, indicating strong complexes were formed.

2.3. Detection of Hg^{2+} with $\text{H}\supset\text{G}$

A series of metal ions including Hg^{2+} , Cu^{2+} , Fe^{3+} , Al^{3+} , Mn^{2+} , Co^{2+} , Sn^{2+} , Cd^{2+} , Ni^{2+} , Au^+ , Ba^{2+} , Ca^{2+} , Ag^+ , K^+ , Fe^{2+} , Mg^{2+} , Pb^{2+} , Na^+ , Zn^{2+} and Cr^{3+} were separately added to $\text{H}\supset\text{G}$ in 100% water. As shown in Figure 4a, only Hg^{2+} gave a notable red-shift from 512 to 528 nm and 538 to 561 nm in UV-vis spectra. Meanwhile, the absorption spectrum became broader and extended to 650 nm. As a result, the solution was transformed from pink to purple, which can be observed by naked eyes (Figure 4c). According to a previous study [42], these changes indicated the formation of a typical charge–transfer complex between $\text{H}\supset\text{G}$ and Hg^{2+} . On the contrary, other metal ions induced absorption intensity change in $\text{H}\supset\text{G}$ to some extent (Figure S7a), but its maximum absorption peaks at 512 and 538 nm showed no obvious red-shift or blue-shift.

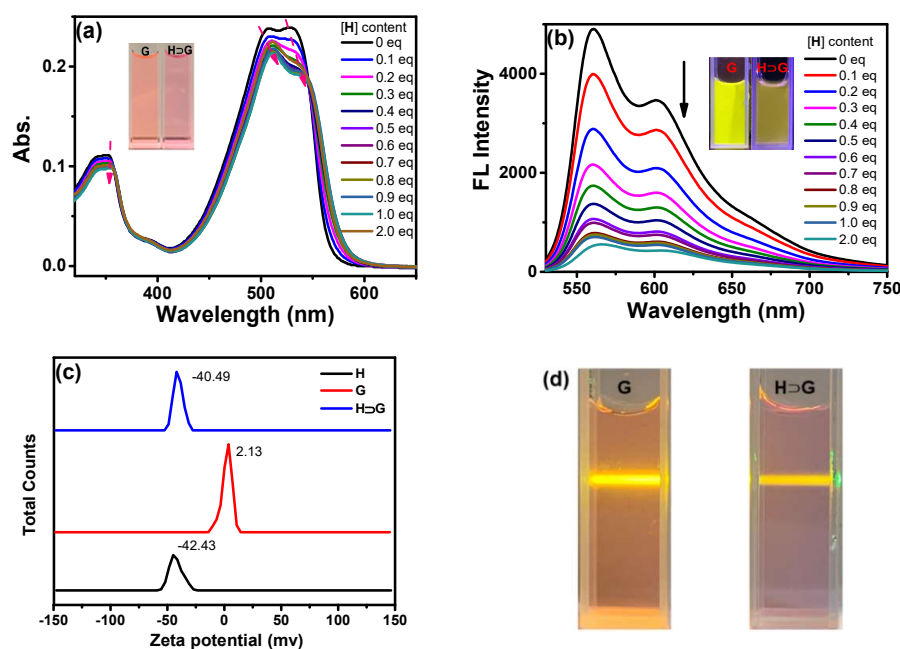


Figure 3. The (a) UV-vis and (b) emission spectra of G aqueous solution in the presence of increasing amounts of H aqueous solution ($[\text{G}] = 10^{-5} \text{ M}$, $\lambda_{\text{ex}} = 510 \text{ nm}$). Insert: Photos of G and $\text{H}\supset\text{G}$ self-assembly under daylight and 365 nm irradiation; (c) The zeta potential of H (10^{-5} M), G (10^{-5} M) and $\text{H}\supset\text{G}$ aqueous solution; (d) The photographs of Tyndall effect of aqueous solution of G and $\text{H}\supset\text{G}$ ($[\text{H}] = 2 \times 10^{-5} \text{ M}$, $[\text{G}] = 10^{-5} \text{ M}$).

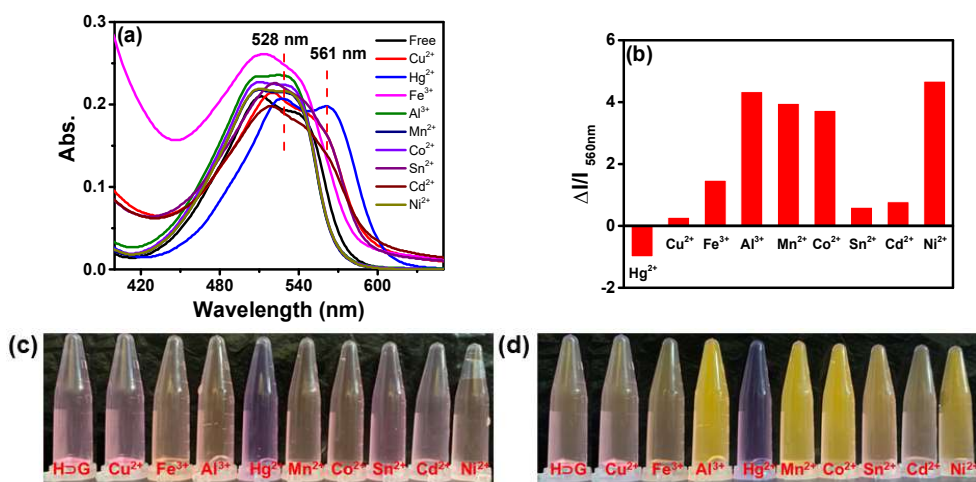


Figure 4. (a) UV-vis and (b) emission spectra of $\text{H}\supset\text{G}$ self-assembly in aqueous solution with the addition of 50 equiv. of different metal ions ($[\text{G}] = 10^{-5} \text{ M}$, $[\text{H}] = 2 \times 10^{-5} \text{ M}$, $\lambda_{\text{ex}} = 510 \text{ nm}$). The photos of $\text{H}\supset\text{G}$ in presence of various metal ions under (c) daylight and (d) 365 nm irradiation.

In addition, only Hg^{2+} could induce the complete fluorescence quenching of HDG . The absolute fluorescence quantum yield of HDG decreased from 3.7% to 0.02% in the absence and presence of 10 equiv. Hg^{2+} . The addition of other metal ions did not lead to fluorescence quenching of HDG . Contrarily, Cu^{2+} , Sn^{2+} , Fe^{3+} , Cd^{2+} gave less than 2-fold fluorescence enhancement. Al^{3+} , Mn^{2+} , Co^{2+} , Ni^{2+} could induce 4–5 fold fluorescence enhancement (Figure 4b,d). As shown in Figure S7b, Ca^{2+} , Mg^{2+} , Ba^{2+} and Pb^{2+} could induce fluorescence enhancement of HDG to a different extent. Fe^{2+} , Ag^+ , Na^+ , Au^+ and K^+ failed to give obvious fluorescence changes in emission spectra. Moreover, the anti-interference experiment indicated the presence of other competing cations did not affect the response of HDG towards Hg^{2+} (Figure S8). Thus, based on UV-vis and emission change in HDG in the presence of Hg^{2+} , the visual and highly selective detection of Hg^{2+} was obtained.

In order to investigate the sensitivity of HDG for Hg^{2+} , fluorescence titration experiments were monitored. The fluorescence emission intensity at 560 gradually decreased with an increase in Hg^{2+} content (Figure 5a). The limit of detection (LOD) of the HDG system for Hg^{2+} was determined to be 7.17×10^{-7} M according to the $3\sigma/K$ method (Figure 5b). The detection performance was similar to or superior to reported pillararenes-based supramolecular systems (Table 1).

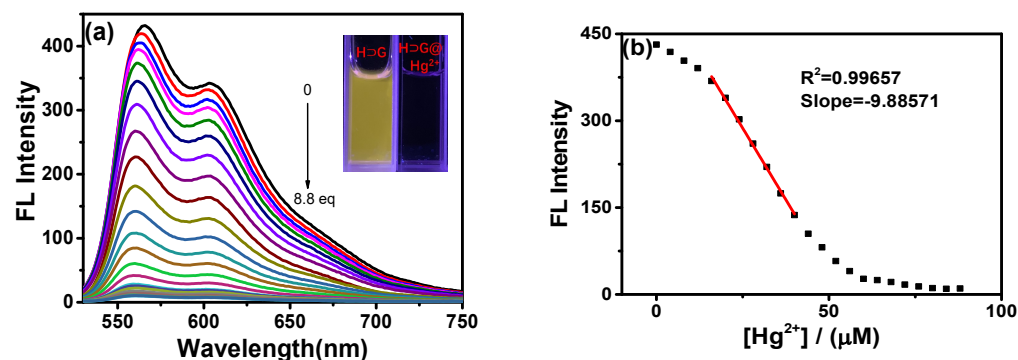
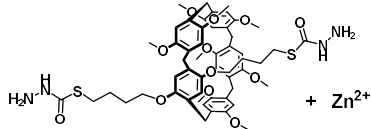
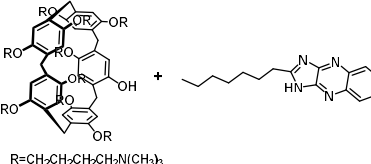
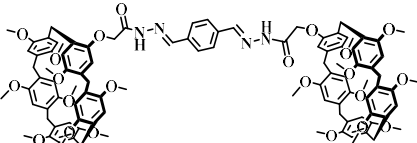
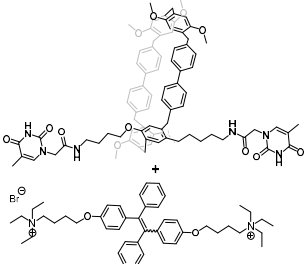
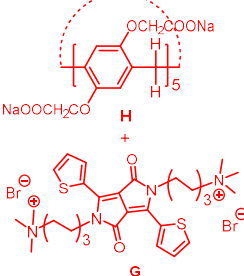


Figure 5. (a) Fluorescence spectra of HDG self-assembly in the presence of increasing amounts of Hg^{2+} ; (b) Plot of fluorescence intensity of HDG self-assembly at 565 nm against the concentration of Hg^{2+} ($\lambda_{\text{ex}} = 510$ nm).

Table 1. The comparison of pillararene-based materials for Hg^{2+} detection.

Pillararene-Based Supramolecular Materials	Detection System, LOD and Sensing Mechanism	Ref.
	DMSO/ H_2O solution (3:7, v/v), LOD = 0.1 μM , coordinated with the O atoms of pillar[5]arene and the N atoms of pyridine groups	[43]
	Acetone, LOD = 2.3 μM , unique T– Hg^{2+} –T pairings between thymine (T) and Hg^{2+}	[18]

Table 1. Cont.

Pillararene-Based Supramolecular Materials	Detection System, LOD and Sensing Mechanism	Ref.
	Metal–organic gel, no LOD data, Fluorescence quenching at 470 nm	[44]
	DMSO/H ₂ O solution (3:7, <i>v/v</i>), LOD = 0.5 μM, fluorescence color change from 545 nm to 502 nm	[45]
	DMSO/H ₂ O (1:1, <i>v/v</i>), LOD = 0.043 μM, Fluorescence quenching at 485 nm, coordination between Hg ²⁺ and probe	[46]
	CHCl ₃ /acetone/H ₂ O (<i>v/v/v</i> = 1:4:495), LOD = 0.03 μM, Unique interaction thymine of G and Hg ²⁺ , Fluorescence turn on at 388 nm.	[21]
	100% water, LOD = 0.7 μM, Fluorescence turn off, interaction with H and N, S atoms of G, removal and separation of Hg ²⁺	This work

2.4. Detection Mechanism of Hg²⁺ with H⊃G

In order to understand the Hg²⁺ detection mechanism by use of H⊃G for such a colorimetric and fluorescence phenomenon, the ¹H NMR spectra of H⊃G in D₂O in the presence of Hg²⁺ were carried out. As shown in Figure 6, proton signals of thienyl (H_a, H_b and H_c) from G showed a slight upfield shift, but H₂, H₃ and H₁ from H showed an obvious upfield shift in the presence of Hg²⁺. In addition to this, the splitting peak of H₁ disappeared, inferring multiple interactions between H⊃G and Hg²⁺ were involved. The ¹H NMR titration spectra suggested that synergistic interactions between Hg²⁺ and host/guest occurred. As we know, the previous work revealed that metal ions could efficiently perturb the microenvironment of host–guest systems [47,48].

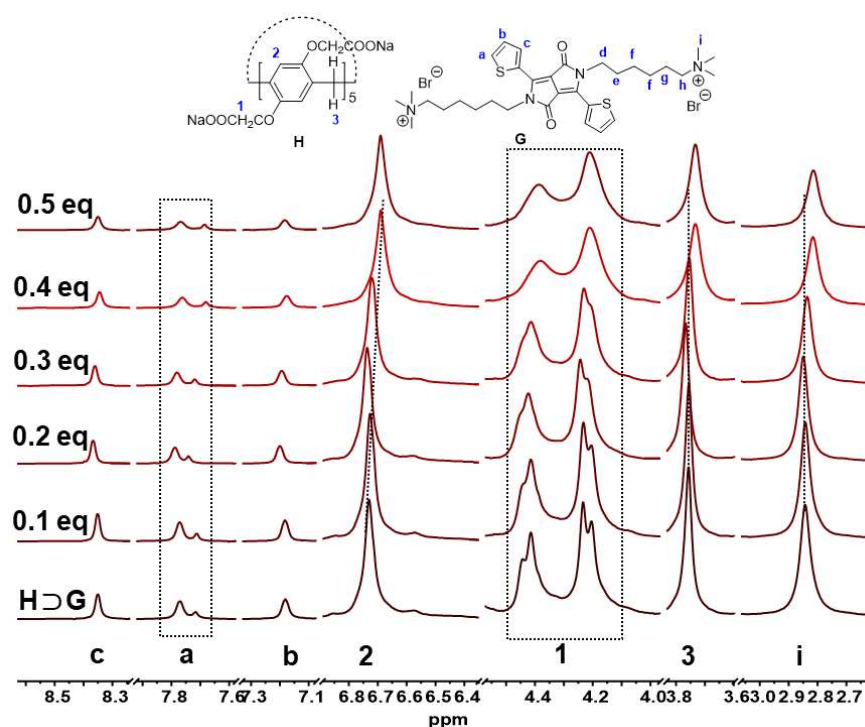


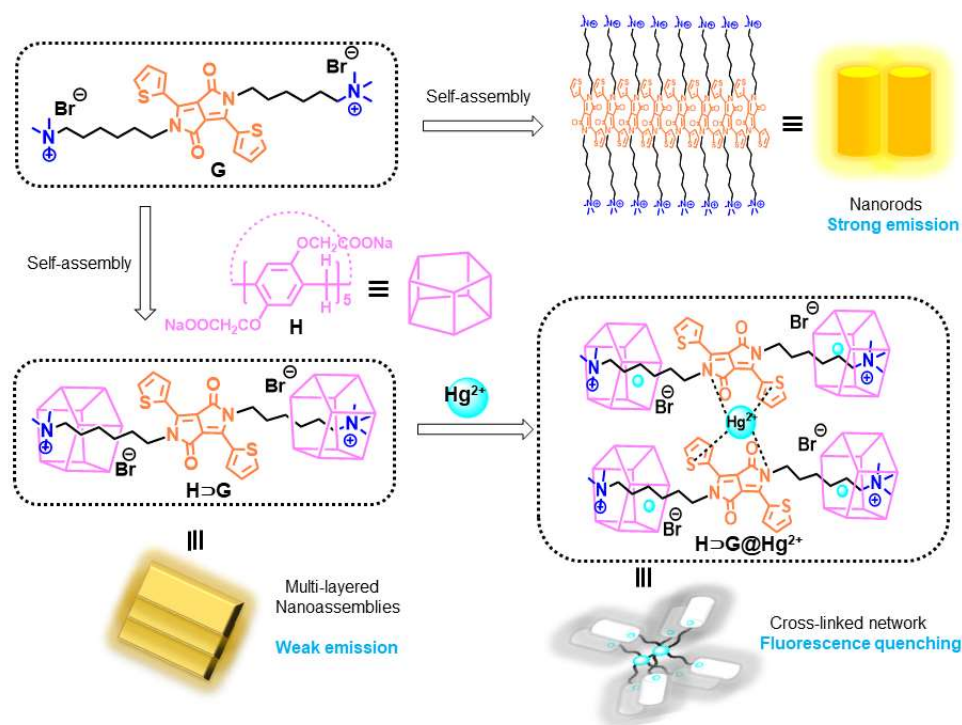
Figure 6. Partial ^1H NMR titration spectra (500 MHz, D_2O) of $\text{H}\supset\text{G}$ ($[\text{G}] = 4 \text{ mM}$, $[\text{H}] = 8 \text{ mM}$) with different equivalents of Hg^{2+} .

At the same time, the control complexation experiment between Hg^{2+} and H or G alone was investigated through ^1H NMR, UV-vis and emission spectra. As shown in Figure S9, for free H , the methylene protons at both rims (H_1) were split into two sets of peaks (4.40 and 4.15 ppm) in a 1:1 integration. However, upon the addition of Hg^{2+} , the peak H_1 was merged into a singlet at 4.20 ppm. Meanwhile, the proton signals from the phenyl moieties (H_2) shifted upfield, and proton signals from the methylene bridge (H_3) changed from a singlet to a broad peak. The distinct changes indicated an interaction between Hg^{2+} and H was present. As shown in Figure S10, ^1H NMR spectra of G showed obvious changes upon the addition of Hg^{2+} . The thienyl and N-CH_2 protons signals of G displayed a down-field shift in sharp contrast with pure G ($\Delta\delta = 0.03, 0.04, 0.03, 0.07 \text{ ppm}$ for protons $\text{H}_c, \text{H}_a, \text{H}_b, \text{H}_d$, respectively), indicating the coordination of Hg^{2+} with S and N atoms of G occurred. The ^1H NMR results were in accordance with a previous study where thienyl DPP could bind to Hg^{2+} with S and N atoms [49]. The presence of Hg^{2+} led to a broad absorption band and an up-shifted baseline of H (Figure S11), indicating Hg^{2+} can be bound inside the electron-rich cavity of H to form an inclusion complex. On the other hand, Hg^{2+} also induced an obvious change in UV-vis spectra of G (Figure S12). As a control, other metal ions failed to take effect on G and H simultaneously (Figures S13 and S14). As shown in Figure S15, $\text{H}\supset\text{G}$ was stable and had excellent detection performance for Hg^{2+} at $\text{pH} < 8$. Upon increase in pH value, $\text{H}\supset\text{G}$ was easy to disassemble due to the hydrolysis of G under alkaline conditions. Therefore, under acidic and neutral conditions, the $\text{H}\supset\text{G}$ complex had a good recognition effect on Hg^{2+} .

Figure S16 shows the Stern–Volmer plot of $\text{H}\supset\text{G}$ quenched by Hg^{2+} . At a low concentration of Hg^{2+} , the quenching efficiency of $\text{H}\supset\text{G}$ was more efficient, and I_0/I vs. the concentration of the quencher gave a linear plot, indicating a static quenching between $\text{H}\supset\text{G}$ and Hg^{2+} was involved.

All these results showed that Hg^{2+} could simultaneously bind G and H by inclusion and coordination interactions, leading to the high selectivity of Hg^{2+} detection with $\text{H}\supset\text{G}$. Namely, as a crosslinking agent, Hg^{2+} induced $\text{H}\supset\text{G}$ to perform self-assembly behavior. SEM images confirmed that a denser and crosslinked network was obtained for $\text{H}\supset\text{G}@ \text{Hg}^{2+}$ (Figure 2e–f), which was different from the multi-layered nanostructure

of HDG . As a result, closer stacking of $\text{H}\text{D}\text{G}@Hg^{2+}$ gave a more pronounced emission quenching effect. The possible Hg^{2+} detection mechanism was shown in Scheme 2.



Scheme 2. Chemical structures and cartoon representations of carboxylatopillar[5]arene sodium salts (**H**) and diketopyrrolopyrrole-bridged bis(quaternary ammonium) guest (**G**) and the schematic representations of their self-assembly in absence and presence of Hg^{2+} in water.

2.5. Reversibility and Application in the Rapid Removal of Hg^{2+}

The reversibility of HDG for Hg^{2+} detection was then evaluated by the addition of Na_2S . As shown in Figure 7a, the presence of Na_2S aqueous solution could easily recover the fluorescence of $\text{H}\text{D}\text{G}@Hg^{2+}$. In addition, with the alternative addition of Na_2S and Hg^{2+} , HDG showed reversible fluorescence changes (Figure 7b). There was no significant loss of the sensitivity and responsiveness of HDG after at least four times. When the HDG -loaded test strip was exposed to Hg^{2+} aqueous solution, an instant change in emission color from yellow to dark was observed. The following S^{2-} treatment gave a fluorescence “turn on” response (Figure 7c). SEM images indicated that a denser and crosslinked network of $\text{H}\text{D}\text{G}@Hg^{2+}@S^{2-}$ was formed (Figure 2g,h).

The interaction between $\text{H}\text{D}\text{G}@Hg^{2+}$ and S^{2-} was assayed by UV-vis spectral changes. As shown in Figure 7d, the absorption band at 561 nm from **G** gradually disappeared, and the band at 292 nm from **H** blue-shifted to 290 nm upon addition of S^{2-} , indicating that multiple interactions were involved between $\text{H}\text{D}\text{G}@Hg^{2+}$ and S^{2-} . As a control, the **H**, **G** and HDG alone further indicated obvious UV-vis spectral responses to S^{2-} (Figure S13a–c). From these results, it can be seen that the presence of S^{2-} served as both Hg^{2+} adsorption agent and crosslinker to $\text{H}\text{D}\text{G}@Hg^{2+}$, leading to a denser and more crosslinked network. As shown in Figure 7e, the distinct UV-vis spectra of HDG , $\text{H}\text{D}\text{G}@Hg^{2+}$ and $\text{H}\text{D}\text{G}@Hg^{2+}@S^{2-}$ were shown.

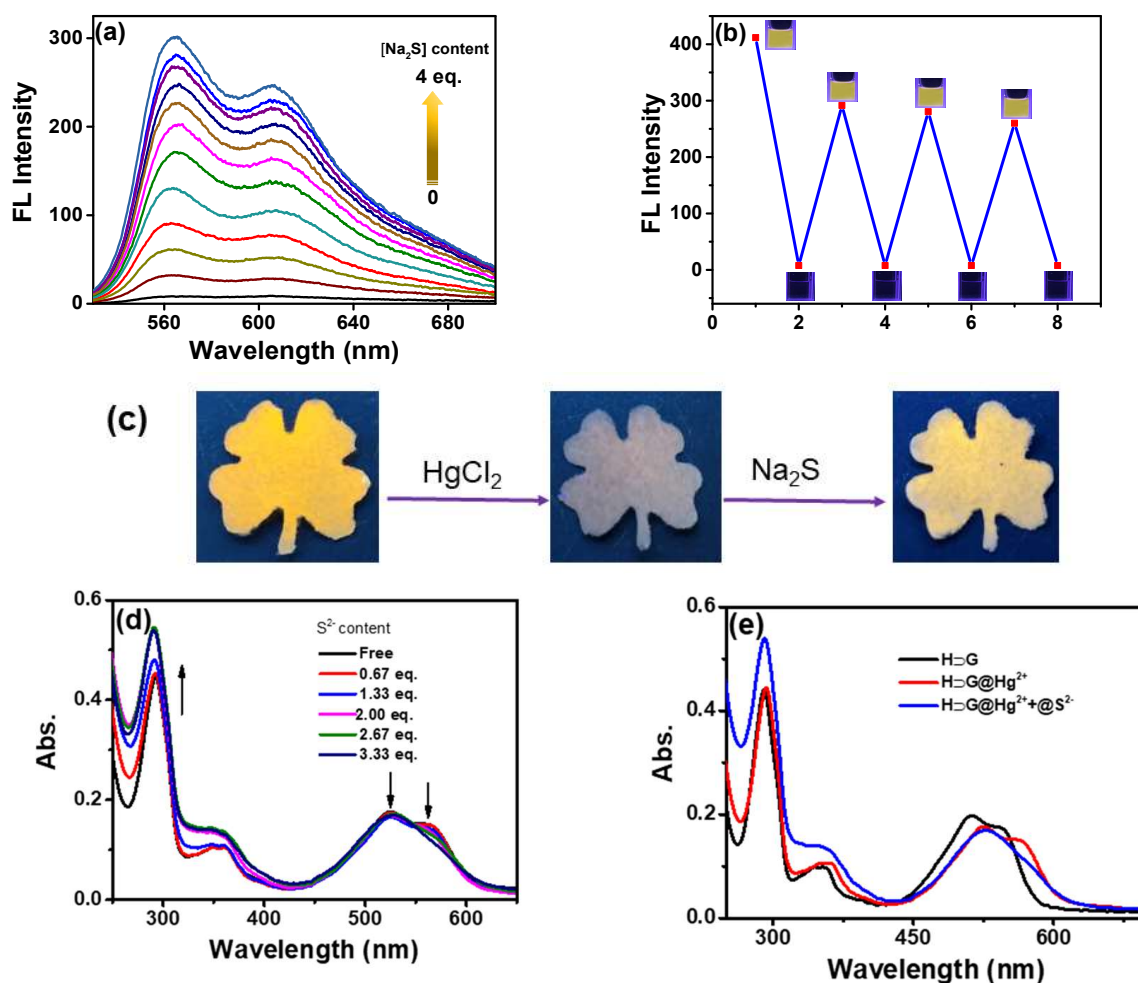


Figure 7. (a) Emission spectra of H₂G@Hg²⁺ self-assembly in the presence of increasing amounts of S²⁻ (from 0 to 4.0 equivalent in aqueous solution); (b) Fluorescent switch of H₂G self-assembly with alternating addition of Hg²⁺ and S²⁻ ($\lambda_{\text{ex}} = 510 \text{ nm}$, $\lambda_{\text{em}} = 560 \text{ nm}$, [H] = $2 \times 10^{-5} \text{ M}$, [G] = 10^{-5} M , [Hg²⁺] = $5 \times 10^{-5} \text{ M}$, [S²⁻] = $2 \times 10^{-4} \text{ M}$); (c) The photos of H₂G-loaded filter paper after exposure of Hg²⁺ and subsequent S²⁻ under 365 nm irradiation; (d) UV-vis spectra of H₂G@Hg²⁺ in the presence of increasing amounts of S²⁻; (e) UV-vis spectra of H₂G, H₂G@Hg²⁺, H₂G@Hg²⁺@S²⁻.

The performance of H₂G in the applicable removal of Hg²⁺ was also investigated. When the aqueous solution of Hg²⁺ (30 ppm in 10 mL water) was added to the mixture of H₂G (100 μM) in water, the apparent black precipitate was present immediately. The resulting mixture was stirred or ultrasound for another 12 h to guarantee the complete adsorption of the Hg²⁺ ion. Then, residual Hg²⁺ content in the mother liquid after centrifugation was measured by inductively coupled plasma (ICP). The Hg²⁺ removal efficiency was found to be 80.78% and 76.85% under stirring and ultrasound, respectively, which was slightly lower than the reported pillararene supramolecular system in organic solvents [18–24]. The possible reason can be ascribed that H₂G@Hg²⁺ has higher solubility in water than in organic solvents, leading to higher Hg²⁺ residual in the mother liquid. Some literature revealed that pillararene could enhance the water dispersibility of insoluble or poorly soluble compounds in water [50,51]. However, in our case, the removal of Hg²⁺ was performed in pure water without any organic solvents, which was greener and more economical. Therefore, H₂G maybe have the potential as a versatile absorbent for Hg²⁺.

In a regeneration treatment, the separated precipitate H₂G@Hg²⁺ was dissolved in 10 mL of water, followed by the addition of an excessive amount of Na₂S, and a black HgS solid was produced. The absorbent H₂G was regenerated and recycled after centrifugation (Figure 8).



Figure 8. Representative photos during the process of sensing and removal of Hg²⁺ and regeneration of absorbent material (H⊃G).

The practical applicability of H⊃G for Hg²⁺ detection was demonstrated by a real sample analysis in tap water and lake water from the South China University of Technology (SCUT). The aliquots of the tap water and lake water were spiked with known amounts of Hg²⁺. As shown in Figure S17, the non-spiked lake water and tap water failed to induce fluorescence change in H⊃G. Upon the presence of Hg²⁺, the emission changes at 560 nm of H⊃G were quenched, which was plotted on the standard calibration curve in Figure 5b, and the recovery of Hg²⁺ was calculated. As shown in Table 2, up 89.7% recovery was obtained, demonstrating the potential applicability of H⊃G for Hg²⁺ detection in the real samples.

Table 2. Detection of mercury ion recovery in lake water and tap water.

Sample	Spiked (μM)	Recovered (μM)	Recovery (%)
Lake Water	20.0	17.4	87.0
	26.7	22.3	83.7
	36.7	31.8	86.7
	40.0	34.7	86.8
Tap water	20.0	16.7	83.6
	26.7	22.5	84.5
	30.0	26.9	89.7
	36.7	31.2	85.2
	40.0	35.6	89.0

3. Conclusions

In summary, a fluorescent supramolecular host–guest system (H⊃G) of water-soluble carboxylatopillar[5]arene sodium salts (H) and a water-soluble DPP derivative (G) was conveniently constructed. Morphological transformation of multi-layered nanostructure was achieved during the addition of H into G aqueous solution, and a fluorescence quenching to some extent was observed. Furthermore, this supramolecular host–guest system (H⊃G) could work as a fluorescent probe to selectively and quantitatively detect Hg²⁺ ions through the formation of crosslinked network H⊃G@Hg²⁺. With the addition of the Hg²⁺ ion, the fluorescence of H⊃G was completely turned off. H⊃G showed a reversible response to Hg²⁺ with a detection limit of 7.17×10^{-7} M. Our work provided pillararene-based supramolecular fluorescent materials not only for fluorescent detection of Hg²⁺ with high selectivity but also for efficient removal of Hg²⁺.

Supplementary Materials: The following supporting information [36,41] can be downloaded at: <https://www.mdpi.com/article/10.3390/bios12080571/s1>, Figure S1: ^1H NMR spectrum (500 MHz, D_2O) of **H**; Figure S2: ^{13}C NMR spectrum (125 MHz, D_2O) of compound **H**; Figure S3: ^1H NMR spectrum (500 MHz, D_2O) of **G**; Figure S4: ^{13}C NMR spectrum (125 MHz, D_2O) of **G**; Figure S5: Normalized UV-vis, emission spectra of **G** in aqueous solution (insert: photographs of aqueous solutions of **G** under daylight and 365 nm light irradiation [G] = 10^{-5} M); Figure S6: Binding isotherm of the **H**⊃**G** complex fitted with a 1:2 binding model according to fluorescence titration experiment ([G] = 10^{-5} M, λ_{ex} = 510 nm); Figure S7: (a) The emission spectra of **H**⊃**G** in presence of different metal ions. (b) Plot of fluorescence intensity changes at 560 nm ($\Delta I/I_0$) in presence of with the addition of 50.0 equiv. in the presence of 50.0 equiv. of other cations in aqueous solution (Hg^{2+} , Cu^{2+} , Fe^{3+} , Al^{3+} , Mn^{2+} , Co^{2+} , Sn^{2+} , Cd^{2+} , Ni^{2+}); Figure S8: ^1H NMR titration spectra (500 MHz, D_2O) of **H** ([**H**] = 8 mM) with different equivalents of Hg^{2+} ; Figure S9: Partial ^1H NMR titration spectra (500 MHz, D_2O) of **G** ([**G**] = 8 mM) upon addition of Hg^{2+} ; Figure S10: UV-vis spectra of **H** upon addition of Hg^{2+} ([**H**] = 10^{-5} M); Figure S11: UV-vis spectra of **G** upon addition of Hg^{2+} ([**G**] = 10^{-5} M); Figure S12: UV-vis spectra of (a) **G** and (b) **H** upon addition of 5 equiv. of different metal ions ([**G**] = [**H**] = 10^{-5} M); Figure S13: UV-vis spectra of (a) **G**, (b) **H** and (c) **H**⊃**G** upon addition of various amount of S^{2-} ([**G**] = [**H**] = 10^{-5} M, for **H**⊃**G**, [**H**] = 10^{-5} M, [**G**] = 2×10^{-5} M).

Author Contributions: X.J.: Investigation, methodology, formal analysis, writing—original draft. L.W.: Conceptualization, Supervision, Validation, Funding acquisition, Writing—review and editing. X.R.: Investigation, Formal analysis. H.T.: Investigation, writing—review and editing. D.C.: Methodology, writing—review and editing. All authors have read and agreed to the published version of the manuscript.

Funding: This research was funded by National Natural Science Foundation of China (22071065) and the Natural Science Foundation of Guangdong Province (2022A1515011743). The APC was funded by 2022A1515011743.

Institutional Review Board Statement: Not applicable.

Informed Consent Statement: Not applicable.

Conflicts of Interest: The authors declare no competing financial interest.

References

1. Mahbub, K.R.; Bahar, M.M.; Labbate, M.; Krishnan, K.; Andrews, S.; Naidu, R.; Megharaj, M. Bioremediation of mercury: Not properly exploited in contaminated soils. *Appl. Microbiol. Biotechnol.* **2017**, *101*, 963–976. [CrossRef]
2. Balali-Mood, M.; Naseri, K.; Tahergorabi, Z.; Khazdair, M.R.; Sadeghi, M. Toxic mechanisms of five heavy metals: Mercury, lead, chromium, cadmium, and arsenic. *Front. Pharmacol.* **2021**, *12*, 643972–643990. [CrossRef]
3. Tchounwou, P.B.; Ayensu, W.K.; Ninashvili, N.; Sutton, D. Review: Environmental exposure to mercury and its toxicopathologic implications for public health. *Environ. Toxicol.* **2003**, *18*, 149–175. [CrossRef]
4. Li, S.X.; Zheng, F.Y.; Yang, H.; Ni, J.C. Thorough removal of inorganic and organic mercury from aqueous solutions by adsorption on Lemna minor powder. *J. Hazard. Mater.* **2011**, *186*, 423–429. [CrossRef]
5. Vendrell, M.; Zhai, D.; Er, J.C.; Chang, Y.-T. Combinatorial strategies in fluorescent probe development. *Chem. Rev.* **2012**, *112*, 4391–4420. [CrossRef]
6. You, L.; Zha, D.; Anslyn, E.V. Recent advances in supramolecular analytical chemistry using optical sensing. *Chem. Rev.* **2015**, *115*, 7840–7892. [CrossRef]
7. Jung, J.H.; Lee, J.H.; Shinkai, S. Functionalized magnetic nanoparticles as chemosensors and adsorbents for toxic metal ions in environmental and biological fields. *Chem. Soc. Rev.* **2011**, *40*, 4464–4474. [CrossRef]
8. Pavase, T.R.; Lin, H.; Shaikh, Q.-U.-A.; Hussain, S.; Li, Z.; Ahmed, I.; Lv, L.; Sun, L.; Shah, S.B.H.; Kalhor, M.T. Recent advances of conjugated polymer (CP) nanocomposite-based chemical sensors and their applications in food spoilage detection: A comprehensive review. *Sens. Actuators B Chem.* **2018**, *273*, 1113–1138. [CrossRef]
9. Dang, Q.-Q.; Wan, H.-J.; Zhang, X.-M. Carbazolic porous framework with tetrahedral core for gas uptake and tandem detection of iodide and mercury. *ACS Appl. Mater. Interfaces* **2017**, *9*, 21438–21446. [CrossRef]
10. Hussain, S.; De, S.; Iyer, P.K. Thiazole-containing conjugated polymer as a visual and fluorometric sensor for iodide and mercury. *ACS Appl. Mater. Interfaces* **2013**, *5*, 2234–2240. [CrossRef]
11. Li, Z.; Yang, Y.W. Macrocyclic-based porous organic polymers for separation, sensing, and catalysis. *Adv. Mater.* **2022**, *34*, 2107401–2107441. [CrossRef] [PubMed]
12. Dai, D.; Yang, J.; Yang, Y. Frontispiece: Supramolecular assemblies with aggregation-induced emission properties for sensing and detection. *Chem. Eur. J.* **2022**, *28*, 202103185–202103198. [CrossRef]

13. Lou, X.-Y.; Song, N.; Yang, Y.-W. A stimuli-responsive pillar[5]arene-based hybrid material with enhanced tunable multicolor luminescence and ion-sensing ability. *Natl. Sci. Rev.* **2021**, *8*, 281–290. [[CrossRef](#)] [[PubMed](#)]
14. Li, J.; Wang, J.; Li, H.; Song, N.; Wang, D.; Tang, B.Z. Supramolecular materials based on AIE luminogens (AIEgens): Construction and applications. *Chem. Soc. Rev.* **2020**, *49*, 1144–1172. [[CrossRef](#)] [[PubMed](#)]
15. Ogoshi, T.; Yamagishi, T.-A.; Nakamoto, Y. Pillar-shaped macrocyclic hosts pillar[*n*]arenes: New key players for supramolecular chemistry. *Chem. Rev.* **2016**, *116*, 7937–8002. [[CrossRef](#)]
16. Cao, D.; Meier, H. Pillararene-based fluorescent sensors for the tracking of organic compounds. *Chin. Chem. Lett.* **2019**, *30*, 1758–1766. [[CrossRef](#)]
17. Jia, Y.; Fang, Y.; Li, Y.; He, L.; Fan, W.; Feng, W.; Yang, Y.; Liao, J.; Liu, N.; Yuan, L. Pillar[5]arenes bearing phosphine oxide pendants as Hg²⁺ selective receptors. *Talanta* **2014**, *125*, 322–328. [[CrossRef](#)]
18. Cheng, H.-B.; Li, Z.; Huang, Y.-D.; Liu, L.; Wu, H.-C. Pillararene-based aggregation-induced-emission-active supramolecular system for simultaneous detection and removal of mercury(II) in water. *ACS Appl. Mater. Interfaces* **2017**, *9*, 11889–11894. [[CrossRef](#)]
19. Roy, S.G.; Mondal, S.; Ghosh, K. Copillar[5]arene-rhodamine conjugate as a selective sensor for Hg²⁺ ions. *N. J. Chem.* **2020**, *44*, 5921–5928. [[CrossRef](#)]
20. Wang, W.M.; Dai, D.H.; Wu, J.R.; Wang, C.Y.; Wang, Y.; Yang, Y.W. Recyclable supramolecular assembly-induced emission system for selective detection and efficient removal of mercury(II). *Chem. Eur. J.* **2021**, *27*, 11879–11887. [[CrossRef](#)]
21. Dai, D.; Li, Z.; Yang, J.; Wang, C.; Wu, J.-R.; Wang, Y.; Zhang, D.; Yang, Y.-W. Supramolecular assembly-induced emission enhancement for efficient mercury(ii) detection and removal. *J. Am. Chem. Soc.* **2019**, *141*, 4756–4763. [[CrossRef](#)] [[PubMed](#)]
22. Zhang, Y.-M.; Zhu, W.; Huang, X.-J.; Qu, W.-J.; He, J.-X.; Fang, H.; Yao, H.; Wei, T.-B.; Lin, Q. Supramolecular aggregation-induced emission gels based on pillar[5]arene for ultrasensitive detection and separation of multianalytes. *ACS Sustain. Chem. Eng.* **2018**, *6*, 16597–16606. [[CrossRef](#)]
23. Lin, Q.; Fan, Y.Q.; Mao, P.P.; Liu, L.; Liu, J.; Zhang, Y.M.; Yao, H.; Wei, T.B. Pillar[5]arene-based supramolecular organic framework with multi-Guest detection and recyclable separation properties. *Chem. Eur. J.* **2018**, *24*, 777–783. [[CrossRef](#)] [[PubMed](#)]
24. Chen, J.-F.; Han, B.-B.; Ma, J.-F.; Liu, X.; Yang, Q.-Y.; Lin, Q.; Yao, H.; Zhang, Y.-M.; Wei, T.-B. Pillar[5]arene-based fluorescent polymer for selective detection and removal of mercury ions. *RSC Adv.* **2017**, *7*, 47709–47714. [[CrossRef](#)]
25. Ma, Y.; Ji, X.; Xiang, F.; Chi, X.; Han, C.; He, J.; Abliz, Z.; Chen, W.; Huang, F. A cationic water-soluble pillar[5]arene: Synthesis and host–guest complexation with sodium 1-octanesulfonate. *Chem. Commun.* **2011**, *47*, 12340–12342. [[CrossRef](#)]
26. Ogoshi, T.; Hashizume, M.; Yamagishi, T.; Nakamoto, Y. Synthesis, conformational and host-guest properties of water-soluble pillar[5]arene. *Chem. Commun.* **2010**, *46*, 3708–3710. [[CrossRef](#)]
27. Hu, X.-Y.; Liu, X.; Zhang, W.; Qin, S.; Yao, C.; Li, Y.; Cao, D.; Peng, L.; Wang, L. Controllable construction of biocompatible supramolecular micelles and vesicles by water-soluble phosphate pillar[5,6]arenes for selective anti-cancer drug delivery. *Chem. Mater.* **2016**, *28*, 3778–3788. [[CrossRef](#)]
28. Chen, L.; Wang, Y.; Wan, Y.; Cai, Y.; Xiong, Y.; Fan, Z.; Conradson, S.D.; Fu, H.; Yuan, L.; Feng, W. Highly efficient and selective pillararene-based organic materials for Hg²⁺ and CH₃Hg⁺ extraction from aqueous solution. *Chem. Eng. J.* **2020**, *387*, 124087–124096. [[CrossRef](#)]
29. Khalil-Cruz, L.E.; Liu, P.; Huang, F.; Khashab, N.M. Multifunctional pillar[*n*]arene-based smart nanomaterials. *ACS Appl. Mater. Interfaces* **2021**, *13*, 31337–31354. [[CrossRef](#)]
30. Chen, L.; Cai, Y.; Feng, W.; Yuan, L. Pillararenes as macrocyclic hosts: A rising star in metal ion separation. *Chem. Commun.* **2019**, *55*, 7883–7898. [[CrossRef](#)]
31. Fang, Y.; Deng, Y.; Dehaen, W. Tailoring pillararene-based receptors for specific metal ion binding: From recognition to supramolecular assembly. *Coord. Chem. Rev.* **2020**, *415*, 213313. [[CrossRef](#)]
32. Shi, B.; Jie, K.; Zhou, Y.; Zhou, J.; Xia, D.; Huang, F. Nanoparticles with near-infrared emission enhanced by pillararene-based molecular recognition in water. *J. Am. Chem. Soc.* **2016**, *138*, 80–83. [[CrossRef](#)] [[PubMed](#)]
33. Gao, L.; Wang, T.; Jia, K.; Wu, X.; Yao, C.; Shao, W.; Zhang, D.; Hu, X.-Y.; Wang, L. Glucose-responsive supramolecular vesicles based on water-soluble pillar[5]arene and pyridylboronic acid derivatives for controlled insulin delivery. *Chem. Eur. J.* **2017**, *23*, 6605–6614. [[CrossRef](#)] [[PubMed](#)]
34. Barbera, L.; Franco, D.; De Plano, L.M.; Gattuso, G.; Guglielmino, S.P.P.; Lentini, G.; Manganaro, N.; Marino, N.; Pappalardo, S.; Parisi, M.F.; et al. A water-soluble pillar[5]arene as a new carrier for an old drug. *Org. Biomol. Chem.* **2017**, *15*, 3192–3195. [[CrossRef](#)]
35. Li, H.; Wei, R.; Yan, G.H.; Sun, J.; Li, C.; Wang, H.; Shi, L.; Capobianco, J.A.; Sun, L. Smart self-assembled nanosystem based on water-soluble pillararene and rare-earth-doped upconversion nanoparticles for pH-Responsive drug delivery. *ACS Appl. Mater. Interfaces* **2018**, *10*, 4910–4920. [[CrossRef](#)]
36. Li, H.; Chen, D.-X.; Sun, Y.-L.; Zheng, Y.B.; Tan, L.-L.; Weiss, P.S.; Yang, Y.-W. Viologen-mediated assembly of and sensing with carboxylatopillar[5]arene-modified gold nanoparticles. *J. Am. Chem. Soc.* **2013**, *135*, 1570–1576. [[CrossRef](#)]
37. Cui, W.; Tang, H.; Xu, L.; Wang, L.; Meier, H.; Cao, D. Pillar[5]arene-diketopyrrolopyrrole fluorescent copolymer: A promising recognition and adsorption material for adiponitrile by selective formation of a conjugated polypseudorotaxane. *Macromol. Rapid Commun.* **2017**, *38*, 1700161. [[CrossRef](#)]

38. Zhou, Y.; Tang, H.; Li, Z.-H.; Xu, L.; Wang, L.; Cao, D. Bio-inspired AIE pillar[5]arene probe with multiple binding sites to discriminate alkanediamines. *Chem. Commun.* **2021**, *57*, 13114–13117. [[CrossRef](#)]
39. Cui, W.; Wang, L.; Xu, L.; Zhang, G.; Meier, H.; Tang, H.; Cao, D. Fluorescent-cavity host: An efficient probe to study supramolecular recognition mechanisms. *J. Phys. Chem. Lett.* **2018**, *9*, 1047–1052. [[CrossRef](#)]
40. Zhang, D.; Cheng, J.; Wei, L.; Song, W.; Wang, L.; Tang, H.; Cao, D. Host–guest complexation of monoanionic and dianionic guests with a polycationic pillararene host: Same two-step mechanism but striking difference in rate upon inclusion. *J. Phys. Chem. Lett.* **2020**, *11*, 2021–2026. [[CrossRef](#)]
41. Liu, Y.; Qu, Z.; Cao, H.Y.; Sun, H.Y.; Gao, Y.; Jiang, X.Y. pH switchable nanoassembly for imaging a broad range of malignant tumors. *ACS Nano* **2017**, *11*, 12446–12452. [[CrossRef](#)]
42. Han, C.; Zhang, Z.; Yu, G.; Huang, F. Syntheses of a pillar[4]arene[1]quinone and a difunctionalized pillar[5]arene by partial oxidation. *Chem. Commun.* **2012**, *48*, 9876–9878. [[CrossRef](#)] [[PubMed](#)]
43. Li, Y.; Lin, Q.; Zhang, Z.; Wei, T.; Shi, B.; Yao, H.; Zhang, Y. In situ formation of Hg²⁺-coordinated fluorescent nanoparticles through a supramolecular polymer network used for efficient Hg²⁺ sensing and separation. *Nanoscale* **2021**, *13*, 9172–9176. [[CrossRef](#)] [[PubMed](#)]
44. Chen, J.; Liu, X.; Ma, J.; Han, B.; Ding, J.; Lin, Q.; Yao, H.; Zhang, Y.; Wei, T. A pillar[5]arene-based multiple-stimuli responsive metal–organic gel was constructed for facile removal of mercury ions. *Soft Matter* **2017**, *13*, 5214–5218. [[CrossRef](#)] [[PubMed](#)]
45. Zhang, Y.; Chen, X.; Liang, G.; Zhong, K.; Lin, Q.; Yao, H.; Wei, T. A novel water soluble pillar[5]arene and phenazine derivative self-assembled pseudorotaxane sensor for the selective detection of Hg²⁺ and Ag⁺ with high selectivity and sensitivity. *New J. Chem.* **2018**, *42*, 10148–10152. [[CrossRef](#)]
46. Lin, Q.; Jiang, X.; Ma, X.; Liu, J.; Yao, H.; Zhang, Y.; Wei, T. Novel bispillar[5]arene-based AIEgen and its' application in mercury(II) detection. *Sensor Actuat. B* **2018**, *272*, 139–145. [[CrossRef](#)]
47. Tseng, T.-W.; Luo, T.-T.; Wu, J.-Y.; Tsai, C.-C.; Huang, C.-Y.; Chiang, M.-H.; Lu, K.-L. Adaptation of guest molecules: A simple system that amplifies the gentle perturbation of host lattices from nickel(II) to cobalt(II). *Inorg. Chim. Acta* **2016**, *445*, 96–102. [[CrossRef](#)]
48. Yao, Q.F.; Lü, B.Z.; Ji, C.D.; Cai, Y.; Yin, M.Z. Supramolecular host-guest system as ratiometric Fe³⁺ ion sensor based on water-soluble pillar[5]arene. *ACS Appl. Mater. Interfaces* **2017**, *9*, 36320–36326. [[CrossRef](#)]
49. Nie, K.; Dong, B.; Shi, H.; Liu, Z.; Liang, B. Thienyl diketopyrrolopyrrole as a robust sensing platform for multiple ions and its application in molecular logic system. *Sens. Actuators B Chem.* **2017**, *244*, 849–853. [[CrossRef](#)]
50. Liu, Y.M.; Chen, X.; Ding, J.M.; Yu, L.; Ma, D.; Ding, J.D. Improved solubility and bioactivity of camptothecin family antitumor drugs with supramolecular encapsulation by water-soluble pillar[6]arene. *ACS Omega* **2017**, *2*, 5283–5288. [[CrossRef](#)]
51. Shangguan, L.; Chen, Q.; Shi, B.; Huang, F. Enhancing the solubility and bioactivity of anticancer drug tamoxifen by water-soluble pillar[6]arene-based host–guest complexation. *Chem. Commun.* **2017**, *53*, 9749–9752. [[CrossRef](#)] [[PubMed](#)]